Multicluster study of the $^{12}C+n$ and $^{12}C+p$ systems

M. Dufour[1,2] and P. Descouvemont[1]
[1]*Physique Nucléaire Théorique et Physique Mathématique, C.P. 229, Université Libre de Bruxelles, B1050 Bruxelles, Belgium*
[2]*Laboratoire de Physique Théorique, Université Louis Pasteur, 23 rue du Loess, F67037 Strasbourg, France*
(Received 25 March 1997)

We use the generator coordinate method to study the $^{12}C(n,\gamma)^{13}C$ and $^{12}C(p,\gamma)^{13}N$ reactions, as well as the ^{13}C and ^{13}N spectroscopy. The ^{12}C wave functions are defined by three α particles in a regular triangle of size R_C. Different configurations are considered, in order to analyze clustering effects. It is shown that spectroscopic properties of ^{13}C and ^{13}N are sensitive to the ^{12}C wave function; reasonable agreement with experiment is found with R_C values minimizing the ^{12}C binding energy. The present study supports the suggestion of a halo structure for the $1/2^+$ excited state in ^{13}C. The neutron and proton capture cross sections are in good agreement with experiment. Finally, we analyze distortion effects in the $^{12}C+n$ wave functions. [S0556-2813(97)02710-6]

PACS number(s): 21.60.Gx, 25.40.Lw, 27.30.+t

I. INTRODUCTION

Many experimental data are available for the $^{12}C+n$ and $^{12}C+p$ systems [1]. In 1952, Thomas [2] analyzed spectroscopic information, nucleon scattering, and capture cross sections. These data, together with new experimental information, were reanalyzed later by Barker and Ferdous [3] in the R-matrix theory. From a consistent fit of many experimental data, Barker and Ferdous investigate spectroscopic properties of low-lying levels of ^{13}C and ^{13}N.

A further interest for the $^{12}C+n$ and $^{12}C+p$ systems comes from astrophysical applications. It is well known that the $^{12}C(p,\gamma)^{13}N$ reaction is the starting point of the CNO cycle, which competes with the pp chain in the hydrogen combustion phase [4]. Although the cross section is relatively well known, extrapolations down to astrophysical energies remain somewhat uncertain. Extrapolations have been done by different authors (for example, Barker and Ferdous [3] use the R-matrix method, Langanke *et al.* [5] use a semimicroscopic two-cluster model).

Recent data by Nagai *et al.* [6] and by Ohsaki *et al.* [7] on the $^{12}C(n,\gamma)^{13}C$ cross section show an unexpected enhancement at astrophysical energies (30 keV). Previous estimates from the cross section at thermal energy gave a cross section at 30 keV much lower than measured. This effect is interpreted [8,9] as a p-wave contribution, quite negligible at thermal energy, but dominant at 30 keV. A potential-model analysis of Mengoni *et al.* [9] shows that matrix elements involved in the cross sections are essentially given by the external contribution for capture to the $^{13}C(1/2^+, E_x=3.09$ MeV) and $^{13}C(5/2^+, E_x=3.85$ MeV) states. These authors suggest a halo structure for the $1/2^+$ state (s wave), bound by 1.86 MeV. This halo structure, characterized by a large spatial extension, should be tested by the $^{12}C(n,\gamma)^{13}C(1/2^+)$ cross section.

As outlined above, the ^{13}C and ^{13}N nuclei cover a broad field of interest. Their study requires a model where bound and scattering states are described in a unified way. In the present work, we use the multicluster generator coordinate method [10] which has been already applied to the $^{12}C(\alpha,\gamma)^{16}O$ [11] and $^{16}O(\alpha,\gamma)^{20}Ne$ [12] reactions. It is well known that ^{12}C is a deformed nucleus, and that a realistic description can be obtained in the α model, with three α particles located at the apexes of a regular triangle (see Ref. [13] and references therein). We use here this triple-α description of ^{12}C to define $^{12}C+n$ and $^{12}C+p$ microscopic wave functions. An advantage of microscopic models is their small number of parameters. When the nucleon-nucleon interaction is chosen, there is no free parameter. This property gives some predictive power to microscopic models, more especially in astrophysical applications where experimental data are often missing or incomplete.

In the present work, we aim at investigating spectroscopic properties of ^{13}C and ^{13}N, and the $^{12}C(n,\gamma)^{13}C$ and $^{12}C(p,\gamma)^{13}N$ reactions in a consistent way, i.e., with the same Hamiltonian and wave functions. We study the importance of deformation effects in the ^{12}C wave functions. The multicluster description of this nucleus allows us to test the sensitivity of the results with respect to the size of ^{12}C. Deformation effects in nucleus-nucleus collisions are poorly known; in the present approach, relative wave functions between ^{12}C and neutron will be analyzed in order to evaluate these effects.

In Sec. II, we present the microscopic cluster model, and give the main formula. Section III is devoted to the spectroscopy of ^{13}C and ^{13}N; different properties, such as rms radii or electromagnetic transition probabilities will be listed. In Sec. IV, we investigate the $^{12}C(p,\gamma)^{13}N$ and $^{12}C(n,\gamma)^{13}C$ capture cross sections. In Sec. V, we show how to derive approximate relative wave functions between ^{12}C and neutron; these wave functions are used to analyze deformation effects of ^{12}C in the $^{12}C+n$ reaction. Concluding remarks are given in Sec. VI.

II. THE MICROSCOPIC MULTICLUSTER MODEL

A. General formalism

We use here the generator coordinate method (GCM, see Ref. [10]) to define the basis wave functions. Details on the GCM can be found in Ref. [14]; its application to multi-

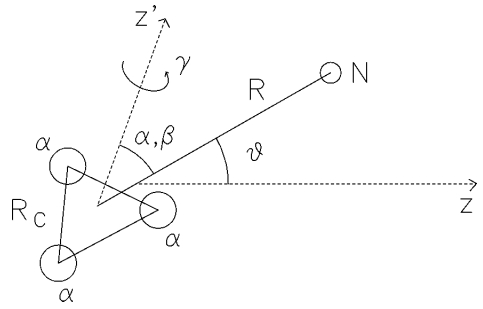

FIG. 1. Cluster structure of the GCM wave functions. Axis z' is perpendicular to the 3α plane.

cluster models is explained in Refs. [15,12]. Here, we only give the main formulas, and emphasize on the peculiarities of the ^{12}C+ nucleon system.

Let us first define the ^{12}C wave functions. They are obtained from α-particle wave functions $\Phi_\alpha(\mathbf{S})$, defined in the harmonic oscillator model and located at $\mathbf{S}$. Here and in the following, all clusters are assumed to have the same oscillator parameter b. A three α wave function is then defined as

$$\Phi_{3\alpha}(R_C,\Omega)=\mathcal{A}\Phi_\alpha(\mathbf{S}_1)\Phi_\alpha(\mathbf{S}_2)\Phi_\alpha(\mathbf{S}_3), \tag{1}$$

where the coordinates $\mathbf{S}_1$, $\mathbf{S}_2$, and $\mathbf{S}_3$ depend on the size of the regular triangle R_C, and on the Euler angles $\Omega=(\alpha,\beta,\gamma)$ (see Fig. 1); $\mathcal{A}$ is the antisymmetrization operator, which ensures that the Pauli principle is correctly taken into account. Rotation and translation invariance of Eq. (1) can be restored [16], yielding a ^{12}C wave function with spin I:

$$\phi_{12}^{I\nu}(R_C)=\phi_{\text{c.m.}}^{-1}\int d\Omega D_{\nu 0}^{I\star}(\Omega)\Phi_{3\alpha}(R_C,\Omega), \tag{2}$$

where $\phi_{\text{c.m.}}^{-1}$ is a center-of-mass wave function, and $D_{\nu 0}^{I}(\Omega)$ is a Wigner function. We assume that the projection of the spin over the intrinsic axis is zero.

Let us now turn to the ^{12}C+ nucleon (N) system; if $\Phi_N^K(\mathbf{S})$ is an s-shell orbital with spin projection K and located at $\mathbf{S}$, the 13-nucleon GCM basis function reads

$$\Phi_{3\alpha+N}^K(\mathbf{R},R_C,\Omega)=\mathcal{A}\Phi_\alpha\left(-\frac{1}{13}\mathbf{R}+\mathbf{S}_1\right)\Phi_\alpha\left(-\frac{1}{13}\mathbf{R}+\mathbf{S}_2\right)\times\Phi_\alpha\left(-\frac{1}{13}\mathbf{R}+\mathbf{S}_3\right)\Phi_N^K\left(\frac{12}{13}\mathbf{R}\right), \tag{3}$$

where $\mathbf{R}$ is the generator coordinate between ^{12}C and the nucleon. As in Eq. (1), $\mathbf{S_1}$, $\mathbf{S_2}$, and $\mathbf{S_3}$ depend on the Euler angles Ω and on R_C. After projection on total spin J and parity π, one has

$$\Phi_l^{JM\pi}(R,R_C)=\phi_{\text{c.m.}}^{-1}\sum_K\langle l1/2\,M-KK|JM\rangle\times\int d\hat{\mathbf{R}}d\Omega Y_l^{M-K}(\hat{\mathbf{R}})\Phi_{3\alpha+N}(\mathbf{R},R_C,\Omega), \tag{4}$$

where l is the relative angular momentum and $\pi=(-)^l$. Notice that we restrict ourselves to ^{12}C states with spin $I=0$. It is well known [17] that a triple-α description of ^{12}C significantly improves the binding energy with respect to the standard one-center description. However, the excitation energy of the 2_1^+ state is underestimated with standard nucleon-nucleon interactions. This yields too strong a coupling between the different channels and, consequently, the ^{12}C(2^+)+nucleon configuration is neglected here.

Equation (4) is written in the GCM approach which involves the Slater determinants (3). This description is well adapted to numerical calculations, but a more intuitive definition is given in the resonating group method (RGM, see Ref. [10]). In RGM notations, Eq. (4) is written as

$$\Phi_l^{JM\pi}(R,R_C)=\sum_K\langle l1/2\,M-KK|JM\rangle\mathcal{A}\phi_{12}(R_C)\times\phi_N^K Y_l^{M-K}(\hat{\boldsymbol{\rho}})\Gamma_l(\rho,R), \tag{5}$$

where $\boldsymbol{\rho}$ is the relative coordinate, $\Gamma_l(\rho,R)$ is a projected Gaussian function [18], and $\phi_{12}(R_C)$ is given by Eq. (2) with $I=\nu=0$. In the following, we shall consider two different approaches: (i) a single R_C value is included in the ^{12}C wave function, which means that the ^{12}C size is frozen for any ^{12}C+ nucleon distance; different R_C values will be considered. (ii) The most realistic approach is to mix several R_C coordinates in the basis states (4). In this way, the ^{12}C nucleus is allowed to be distorted during the collision.

B. Wave functions without distortion

In this case, the ^{12}C + nucleon system is described with a single R_C value. The total wave function reads

$$\Psi_{R_C,l}^{JM\pi}=\sum_R f_{R_C,l}^{J\pi}(R)\Phi_l^{JM\pi}(R,R_C), \tag{6}$$

where $f_{R_C,l}^{J\pi}(R)$ is the generator function, deduced from matrix elements of the Hamiltonian between basis states (4) (see Ref. [14] for details). Typically 10 generator coordinates are included in the summation.

In RGM notations, Eq. (6) is written as

$$\Psi_{R_C,l}^{JM\pi}=\sum_K\langle l1/2\,M-KK|JM\rangle\mathcal{A}\phi_{12}(R_C)\times\phi_N^K Y_l^{M-K}(\hat{\boldsymbol{\rho}})g_l^{J\pi}(\rho), \tag{7}$$

where the radial function is given by

$$g_l^{J\pi}(\rho)=\sum_R f_{R_C,l}^{J\pi}(R)\Gamma_l(\rho,R). \tag{8}$$

C. Wave functions with distortion

A natural extension of Eq. (6) is

$$\Psi_l^{JM\pi}=\sum_{R,R_C}F_l^{J\pi}(R_C,R)\Phi_l^{JM\pi}(R,R_C), \tag{9}$$

where a coupling between different R_C values is now introduced. This definition is quite valid for spectroscopy, where boundary conditions can be neglected. However, extension

of (6) with a sum over R_C would introduce nonorthogonal channels, corresponding to different values of R_C. To solve this problem, the ^{12}C basis is first diagonalized, yielding

$$\phi_{12}^{\omega}=\sum_{R_C} c^{\omega}(R_C)\phi_{12}(R_C), \tag{10}$$

where functions ϕ_{12}^{ω} are orthogonal to each other; $\omega=0$ corresponds to the ^{12}C ground state, whereas $\omega\neq 0$ corresponds to pseudostates [19] well known in multicluster approaches [15], or in two-cluster studies with monopole distortion [20]. In this new basis, the total wave function (9) reads, in RGM notations,

$$\Psi_l^{JM\pi}=\sum_{\omega,K}\langle l1/2\, M-KK|JM\rangle \mathcal{A}\phi_{12}^{\omega}\phi_N^K Y_l^{M-K}(\hat{\boldsymbol{\rho}})g_{\omega,l}^{J\pi}(\rho). \tag{11}$$

In this way, channels corresponding to different ω values are asymptotically orthogonal, as required in scattering studies; ω values different from zero do not have physical interpretation, but are considered as distortion channels, which allow deformation of ^{12}C during the collision. Notice that the GCM expansions (6) and (9) are not valid for large relative coordinates. Indeed, the asymptotic behavior of Gaussian functions is adapted neither to scattering states nor to bound states. This problem is solved in the microscopic R-matrix method (MRM, see Refs. [18,14]). The calculation of the wave functions (6) or (9) requires the calculation of matrix elements between projected Slater determinants. For ^{12}C basis states (2), this calculation involves three-dimensional integrals, as explained in Ref. [13]. Matrix elements between 13-nucleon GCM functions (4) involve seven-dimensional integrals; the principle of the calculation is given in Ref. [12] and is not repeated here. Let us however point out that this numerical calculation is highly time consuming, owing to the multiple angular-momentum projection. Therefore, special attention must be paid on the optimization of the computer codes.

III. SPECTROSCOPY OF ^{13}C AND ^{13}N

A. Properties of ^{12}C

As a preliminary study, we investigate the properties of ^{12}C as a function of R_C. According to Ref. [13], the oscillator parameter is $b=1.38$ fm. Here and in the following, we use two different nucleon-nucleon potentials: the V2 Volkov potential [21] and the Minnesota potential [22]. Both interactions involve a parameter (m and u, respectively) whose standard values are $m=0.6$ and $u=1$. With these forces, the α binding energy is -27.96 MeV and -24.06 MeV, respectively. The spin-orbit force does not contribute in the α model. In Fig. 2, we show the binding energy of the ^{12}C ground state for both potentials. In addition to the standard parameters, potentials with $m=0.578$ and $u=0.901$, which will be used for ^{13}C, are also shown. As is well known, the minima of the binding energy are located at R_C values significantly different from zero. However, the precise location is rather sensitive to the interaction. For the standard parameters, the V2 potential gives $R_C=2.7$ fm at the minimum,

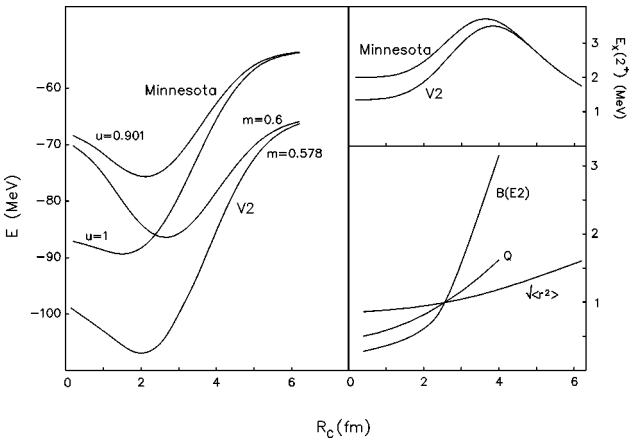

FIG. 2. Left panel: binding energy of the ^{12}C ground state as a function of R_C. The curves are labeled by the u (or m) parameter for the Minnesota (or Volkov) forces. Right upper panel: Excitation energy of the 2^+ state. Right lower panel: ground-state rms radius, 2^+ quadrupole Q moment, and $B(E2,2^+\rightarrow 0^+)$ normalized to the experimental values (2.46 fm, 6 ± 3 e fm^2 and 4.65 ± 0.26 W.u., respectively [23]).

whereas the Minnesota potential $R_C=1.6$ fm. When the parameters are fitted to the ^{13}C energy, both potentials present a minimum near $R_C=2.0$ fm.

The right panel shows the 2^+ excitation energy, whose experimental values (4.44 MeV) cannot be obtained for any ^{12}C configuration. The best agreement (≈ 3.3 MeV) is obtained for R_C close to 4 fm, which is far from the minimum of the ground-state binding energy. The rms radius of the ground state, the quadrupole moment of the 2^+ state, and the $B(E2)$ between those states are also analyzed as a function of R_C. For convenience, they are normalized to the experimental values [23]. The GCM results do not depend on the nucleon-nucleon interaction, since a single configuration is taken into account. For the rms radius, the R_C value corresponding to experiment is $R_C=2.7$ fm (notice that the GCM radii have been corrected to take account of the proton radius 0.8 fm). If we consider the error bar, the experimental quadrupole moment is reproduced roughly from $R_C=1$ fm to $R_C=4$ fm. For the $B(E2,2^+\rightarrow 0^+)$, R_C values close to 2.7 fm are also consistent with the experimental value. Even if one considers that these results are obtained within a single model of a single generator coordinator, all spectroscopic properties are consistent with an important deformation of ^{12}C and with a triangle size close to 2.7 fm.

B. Properties of ^{13}C and ^{13}N

In order to study the influence of clustering in ^{13}C and ^{13}N, we consider two approaches: (i) the $^{12}C+$ nucleon wave functions involve a single R_C value ($R_C=0.4$, 1.4, 2.7, and 4.0 fm are used), and (ii) the ^{12}C nucleus involves a mixing of three R_C values ($R_C=1.4$, 2.7, and 4.0 fm). The relative motion between ^{12}C and the nucleon is described by six generator coordinates $R=2.0$ fm to 9.0 fm with a step of 1.4 fm. A spin-orbit force [24] with strength $S_0=30$ MeV fm^5 is included in the Hamiltonian.

Since we are interested in spectroscopic properties which are sensitive to the energy, we determine the nucleon-nucleon interaction for both parities. In Table I, we give the

TABLE I. Parameters m and u of the Volkov and Minnesota interactions.

^{13}C	R_C=0.4	R_C=1.4	R_C=2.7	R_C=4.0	Mixed
$m(+)$	0.538	0.525	0.517	0.528	0.532
$m(-)$	0.641	0.623	0.537	0.420	0.578
$u(+)$	1.044	1.077	1.113	1.092	1.054
$u(-)$	0.777	0.829	1.072	1.421	0.901
^{13}N	R_C=0.4	R_C=1.4	R_C=2.7	R_C=4.0	Mixed
$m(+)$	0.545	0.534	0.531	0.538	0.542
$m(-)$	0.639	0.621	0.538	0.428	0.578
$u(+)$	1.041	1.070	1.088	1.077	1.047
$u(-)$	0.783	0.833	1.071	1.407	0.903

m and u values which reproduce the $1/2^+_1$ excitation energy for positive parity, and the ground-state energy (with respect to ^{12}C) for negative parity. It is interesting to compare the parameters of $R_C=0.4$ fm (equivalent to a usual two cluster model) to those of the full calculation. Whereas the former approach yields rather different parameters for both parities, the latter involves much closer parameters, for both potentials. Although there is still a slight parity effect, the multicluster model is an improvement in this direction.

The energy spectra with the full ^{12}C basis are presented in Fig. 3. The $3/2^-$ excitation energy is always too low with respect to experiment; this problem might be due to the lack of $S\geqslant\frac{1}{2}$ components in the wave functions. The $5/2^+$ state is reasonably well described for both potentials.

Let us now discuss some spectroscopic properties, which are shown in Table II.

Proton widths in ^{13}N. The total width of the $1/2^+$ ($E_{\text{c.m.}}=0.42$ MeV) resonance in ^{13}N is somewhat overestimated. The overestimation factor is, however, lower for the Minnesota potential. For the $3/2^-$ state ($E_{\text{c.m.}}=1.56$ MeV) we present the reduced width (calculated at 9.0 fm) since the total width is very sensitive to the energy, not fitted by the potential. The conclusions are similar to those of the $1/2^+$ resonance.

rms radii in ^{13}C. The ground-state charge radius is known to be 2.46 fm [1]. However radius determination is often model dependent, and this value is contradicted by the neutron radius (2.35 fm) which is expected to be slightly larger than the proton radius. Our results do not strongly depend on the interaction; in the full basis, we get rms radii somewhat lower than experiment (2.36 fm for V2 and 2.30 fm for Minnesota).

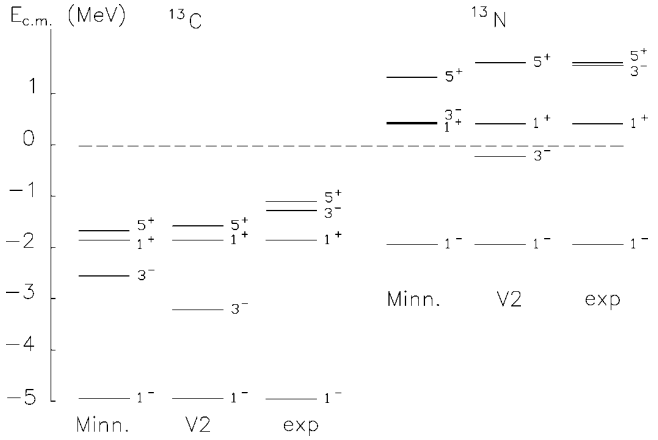

FIG. 3. Energy spectra of ^{13}C and ^{13}N. The states are labeled by $2J$. Experimental data are taken from Ref. [1].

Interest for the spectroscopy of the $1/2^+$ excited state has been raised by its possible halo structure [8,9]. This exotic structure, characterized by large rms radii, is mainly found in core + neutron(s) systems with low binding energy and s-wave neutrons. To investigate the $1/2^+$ structure, we present the mean distance d between the ^{12}C core and the external neutron. This quantity is defined from

$$13\langle r^2\rangle_{13}=12\langle r^2\rangle_{12}+\frac{12}{13}d^2, \tag{12}$$

where $\langle r^2\rangle_{12}$ and $\langle r^2\rangle_{13}$ are the ^{12}C and ^{13}C rms radii, respectively. The values obtained in Table II are weakly dependent on the ^{12}C wave function or on the nucleon-nucleon interaction. It is in every case much larger than the ^{12}C radius (for comparison, this quantity in the ground state is about 1–2 fm). Although smaller than in well known halo nuclei such as ^{11}Be or ^{11}Li, this distance d supports the existence of a halo structure in the ^{13}C($1/2^+$) state. Further analysis will be given by the wave functions (see Sec. V).

Electromagnetic transition probabilities. Experimental values for the $B(E1,1/2^+\rightarrow 1/2^-)$ in ^{13}C and ^{13}N are rather different (0.039 ± 0.004 W.u. and 0.10 ± 0.01 W.u., respectively) although charge symmetry would yield similar results. This difference has been interpreted by Barker and Ferdous [3] as a manifestation of charge-symmetry breaking, due to different asymptotic behavior of the wave functions. The present model is consistent with a reduction of the $E1$ transition probability in ^{13}C, but lower than experiment. Obviously, the precise values of the matrix elements are sensitive to small details of the wave functions [3] which cannot be reproduced in a parameter-free model. The same phenomenon occurs for the $3/2^-\rightarrow 1/2^+$ transition, where charge-symmetry breaking is better reproduced by the GCM. All these $E1$ transition probabilities are very sensitive to the ^{12}C description. A two-cluster model ($R_C\approx 0$) would strongly overestimate the experimental values. The improvement brought by a multicluster approach is also exemplified by the $B(E2,3/2^-\rightarrow 1/2^-)$ transition probability in ^{13}C; values of R_C close to 3.5 fm are necessary to reproduce the experimental data. Notice that the transition probabilities are weakly sensitive to the choice of the nucleon-nucleon interaction, and also to the precise energies of the states. The $1/2^+ - 3/2^-$ ordering, which is uncorrectly predicted by the model, has a weak influence on the $B(E1)$. Numerical simulations have been done by changing the $3/2^-$ interaction to fit the experimental energy. The $B(E1)$ value is modified by a few percent only.

$^{12}C+n$ scattering length. The scattering length a is obtained from the s phase shift δ as

$$a=-\lim_{k\rightarrow 0}\frac{1}{k}\tan\,\delta(k), \tag{13}$$

TABLE II. ^{13}C and ^{13}N properties. Reduced transition probabilities are expressed in W.u., the scattering length a [Eq. (13)], the rms radius $\langle r^2\rangle$ and the distance d [Eq. (12)] are expressed in fm. The dimensionless reduced width θ^2 is calculated at 9 fm. The first and second lines correspond to the V2 and Minnesota interactions, respectively.

^{13}C	$R_C=0.4$	$R_C=1.4$	$R_C=2.7$	$R_C=4.0$	Mixed	Expt.[a]
$B(E1,1/2^+\rightarrow 1/2^-)$	0.17	0.17	0.07	2.1×10^{-3}	0.104	0.039±0.004
	0.15	0.16	0.047	1.8×10^{-3}	0.103	
$B(E1,3/2^-\rightarrow 1/2^+)$	0.28	0.20	0.059	8.0×10^{-3}	0.094	0.039±0.006
	0.22	0.16	0.034	8.5×10^{-5}	0.091	
$B(E2,3/2^-\rightarrow 1/2^-)$	1.0	1.0	2.8	3.8	2.2	3.5±0.8
	1.1	1.6	2.9	3.7	2	
a	6.51	6.66	7.08	6.92	6.68	6.65
	6.23	6.40	6.97	6.73	6.37	
$\sqrt{\langle r^2\rangle}(1/2^-)$	2.19	2.26	2.50	2.92	2.36	2.46
	2.19	2.26	2.49	2.91	2.30	
$d(1/2^+)$	4.63	4.71	4.96	4.66	4.71	
	4.39	4.48	4.83	4.46	4.48	
^{13}N	$R_C=0.4$	$R_C=1.4$	$R_C=2.7$	$R_C=4.0$	Mixed	Expt.[a]
$B(E1,1/2^+\rightarrow 1/2^-)$	0.21	0.2	0.11	0.02	0.136	0.10±0.01
	0.18	0.18	0.071	6.5×10^{-4}	0.128	
$B(E1,3/2^-\rightarrow 1/2^+)$	0.56	0.31	0.088	0.031	0.144	0.1
	0.44	0.25	0.052	6.9×10^{-3}	0.136	
$\Gamma_p(1/2^+)$ (keV)	35.6	39.9	43.1	38.4	40.2	31.7±0.8
	31.2	32.8	41.7	36.1	34.2	
$\theta^2(3/2^-)(\%)$	6.1	6.2	7.6	10.2	7.3	2.9±0.2
	4.1	4.6	5.4	7.2	4.8	

[a]Reference [1].

where k is the wave number. This quantity is almost independent on the ^{12}C wave function; all results are consistent with the experimental values $a=6.65$ fm. This means that low-energy scattering wave functions are weakly sensitive to the ^{12}C description.

IV. CAPTURE CROSS SECTIONS ON ^{12}C

A. The $^{12}C(p,\gamma)^{13}N$ cross section

In Fig. 4, we present the $^{12}C(p,\gamma)^{13}N$ S factor obtained with the full ^{12}C basis, and for the V2 and Minnesota poten-

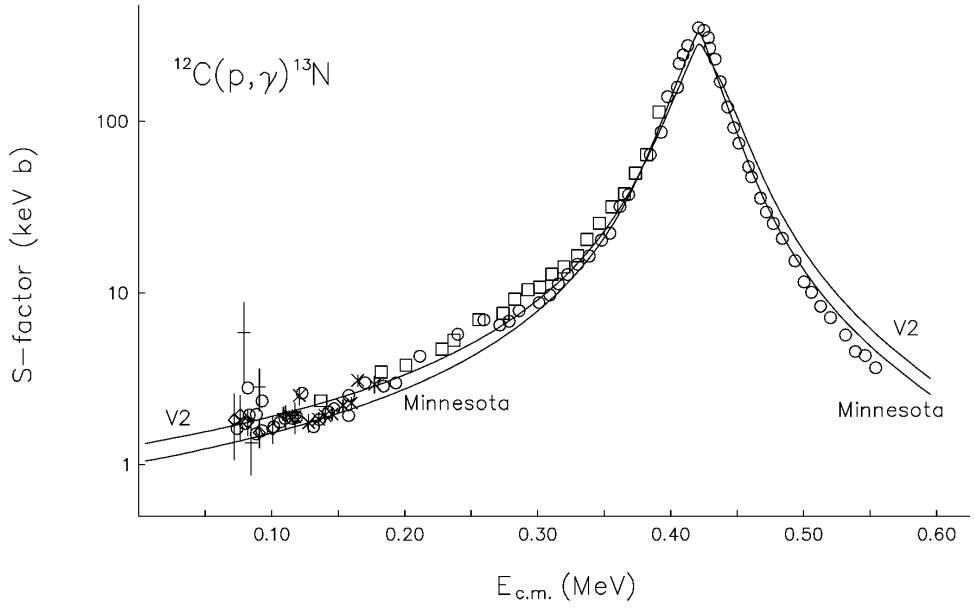

FIG. 4. $^{12}C(p,\gamma)^{13}N$ S factor as a function of the c.m. energy. Experimental data are from Refs. [25] (○), [26] (□), [27] (+), [28] (×), and [29] (◇).

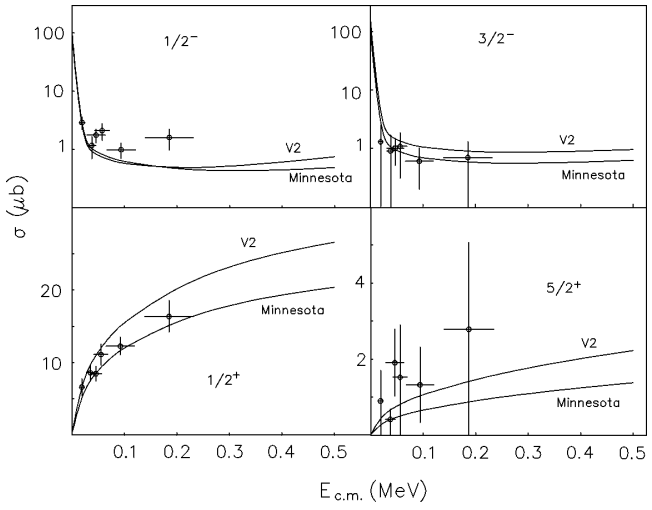

FIG. 5. $^{12}C(n,\gamma)^{13}C$ cross sections corresponding to the different ^{13}C bound states. The data are from Ref. [6].

tials. This cross section is mainly given by the properties of the $1/2^+$ ($E_{\text{c.m.}}=0.42$ MeV) resonance. However, the low-energy tail is sensitive to a background component which distorts the S factor from a pure Breit-Wigner approximation. As expected from Table II, the peak obtained with the V2 interaction is slightly too broad, since the experimental proton width is overestimated by 20%. This factor is however compensated by a similar overestimation in the γ width. Below the resonance energy, both theoretical curves are consistent with the data, which indicates that the background component is realistic. At zero energy, we have $S(0)=1.0$ keV b for the Minnesota potential, and $S(0)=1.3$ keV b for the V2 potential. These values are slightly lower than those used in astrophysics [30] [$S(0)=1.4$ keV b].

B. The $^{12}C(n,\gamma)^{13}C$ cross sections

Cross sections corresponding to the four bound states of ^{13}C are given in Fig. 5. Since low-energy cross sections are sensitive to the asymptotic behavior of the wave functions, parameters u or m of the Minnesota or Volkov potentials have been slightly modified for the $3/2^-$ and $5/2^+$ bound states in order to reproduce the experimental binding energies. Figure 5 indicates that the overall agreement between GCM and experiment is fairly good. In each case, the V2 interaction yields cross sections slightly larger than the Minnesota interaction. As expected, $1/2^-$ and $3/2^-$ cross sections are determined by the $l=0$ partial wave, yielding a $E^{-1/2}$ energy dependence; on the contrary, the $1/2^+$ and $5/2^+$ components are mainly given by p waves and hence are characterized by an $E^{1/2}$ energy dependence.

The thermal cross section is $\sigma_{\text{th}}=3.09$ mb for the V2 potential and 2.57 mb for the Minnesota potential, in reasonable agreement with experiment (3.53 ± 0.07 mb, see Ref. [1]). However the experimental branching ratios (67.5% for the ground state and 32.4% for the $3/2^-$ excited state) are poorly reproduced (37.1% and 62.9% for V2 and 50.2% and 49.8% for Minnesota respectively).

Capture cross section to the $1/2^+$ state has been checked to be rather sensitive to the asymptotic parts of the wave function, as suggested by Mengoni *et al.* [9]. The good agreement with the data supports the validity of the model for the $1/2^+$ structure. Therefore, the large distance between ^{12}C and neutron (see Table II), and hence the halo structure, should be reliable.

V. DISTORTION EFFECTS IN THE $^{12}C+n$ SYSTEM

A. Energy curves

There are different ways to investigate distortion of ^{12}C in the $^{12}C+n$ system. We should first emphasize that deformation of ^{12}C is possible only when different R_C values are included in the GCM basis. When a single R_C value is used, the ^{12}C nucleus has a fixed size which is identical for any $^{12}C+n$ distance. Let us first consider the energy curves defined as

$$E_l^{J\pi}(R_C,R)=\frac{H_l^{J\pi}(R_C,R;R_C,R)}{N_l^{J\pi}(R_C,R;R_C,R)}-E_{12}(R_C)-\frac{1}{4}\hbar\omega, \tag{14}$$

where $E_{12}(R_C)$ is the ^{12}C energy, and $\hbar\omega/4$ is the residual kinetic energy which ensures that the energy curves tend to zero for large R. In Eq. (14), $H_l^{J\pi}$ and $N_l^{J\pi}$ are the Hamiltonian and overlap kernels defined as

$$\begin{Bmatrix} H_l^{J\pi}(R_C,R;R_C',R') \\ N_l^{J\pi}(R_C,R;R_C\prime,R') \end{Bmatrix} = \left\langle \Phi_l^{J\pi}(R,R_C)\left|\begin{Bmatrix} H \\ 1 \end{Bmatrix}\right|\Phi_l^{J\pi}(R',R_C')\right\rangle, \tag{15}$$

where $\Phi_l^{J\pi}$ are the projected Slates determinants (4). It is well known that the energy curves (14) are not genuine nucleus-nucleus potentials, but they give a qualitative insight on the system.

In Fig. 6, we show on the upper panels, the energy curves (14) for the $1/2^-$ ground state and the $1/2^+$ excited state (here and in the following, the V2 potential is used). In the ground state, the barrier height increases when R_C is small, which means that $^{12}C+n$ clustering is sensitive to the R_C value. The same conclusion holds for the $1/2^+$ state, where the minimum location is pushed towards large R values when R_C increases. This effect was already observed in the $\alpha+{}^{12}C$ system [15]. Notice however that calculations with $R_C=4.0$ fm are not quite realistic, but are used to illustrate situations involving strongly deformed nuclei. The upper panel represents each system with an adjusted nucleon-nucleon interaction. In the lower panel, we consider the full basis calculation, where the energy curves labeled ''mixed'' are defined by the eigenvalue problem

$$\sum_{R_C'}\left[H_l^{J\pi}(R_C,R;R_C',R)-E_l^{J\pi}(R)N_l^{J\pi}(R_C,R;R_C',R)\right] \times d_{l\omega}^{J\pi}(R_C')=0, \tag{16}$$

where the excitation level refers to $\omega=0$.

Figure 6 shows that $R_C=4.0$ fm components have a rather high energy, and are weakly coupled with the other values. The role of this configuration is mainly in the ^{12}C spectro-

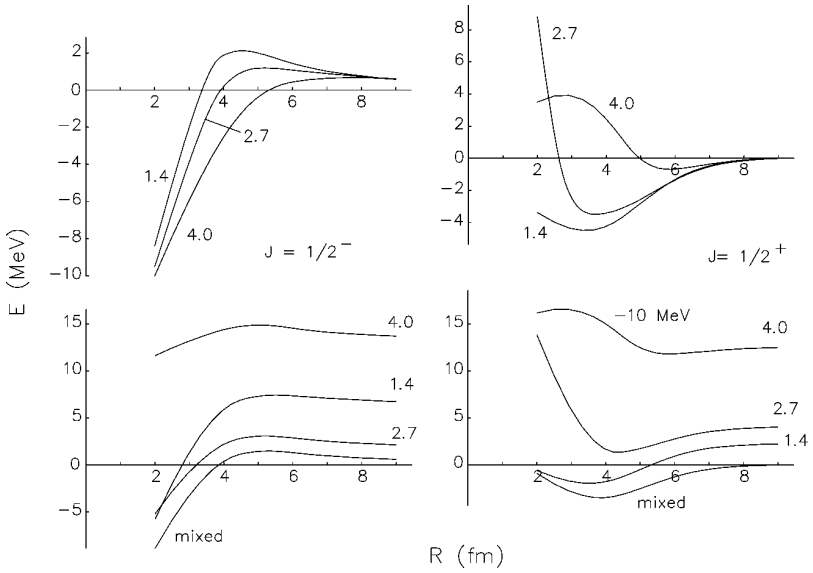

FIG. 6. $^{12}C+n$ energy curves [Eq. (14)]. The upper panels refer to calculations with a single ^{12}C configuration (with the interaction fitted individually, see Table I). The lower panels refer to the multiconfiguration approach.

scopic properties. Since the $1/2^-$ and $1/2^+$ partial waves have different parameters in the nucleon-nucleon interaction (see Table I), the lowest energy curve is different ($R_C=2.7$ fm for $1/2^-$ and $R_C=1.4$ fm for $1/2^+$). In both cases, the mixing of different R_C improves the energy by about 2 MeV.

B. Wave functions

The relative wave functions $g^{J\pi}(\rho)$ involved in Eqs. (7) and (11) cannot be directly interpreted without the antisymmetrizer operator $\mathcal{A}$ [10,31]. These functions are not orthogonal to each other and, in two-center calculations (or for small R_C values in multicluster models) they are known to be affected by the so-called ''Pauli forbidden states.''

It is however possible to derive an approximate relative function $\hat{g}^{J\pi}_{\omega,l}(\rho)$ such that Eq. (11) can be rewritten as

$$\Psi^{JM\pi}_l \approx \sum_\omega \phi^\omega_{12}[\phi_N \otimes Y_l(\hat{\boldsymbol{\rho}})]^{JM} \hat{g}^{J\pi}_{\omega,l}(\rho), \tag{17}$$

i.e., *without* the antisymmetrizer operator. This expression allows a more intuitive analysis of the wave function; it is the starting point of the orthogonality condition model [33]. The wave function $\hat{g}^{J\pi}_{\omega,l}(\rho)$ is derived from [32,10,31]

$$\hat{g}^{J\pi}_{\omega,l}(\rho) = \mathcal{N}^{1/2} g^{J\pi}_{\omega,l}(\rho), \tag{18}$$

where $\mathcal{N}$ is the RGM overlap kernel. As usual, $\mathcal{N}^{1/2}$ is expanded on the eigenstates $\chi^{J\pi}_{ln}$, yielding

$$\hat{g}^{J\pi}_{\omega,l}(\rho) = \sum_n (\mu^{J\pi}_{ln})^{1/2} \langle g^{J\pi}_{\omega,l} | \chi^{J\pi}_{ln} \rangle \chi^{J\pi}_{ln}, \tag{19}$$

where $\mu^{J\pi}_{ln}$ are the eigenvalues of the overlap kernel

$$\mathcal{N}\chi^{J\pi}_{ln} = \mu^{J\pi}_{ln} \chi^{J\pi}_{ln}. \tag{20}$$

To determine the eigenvalues and eigenfunctions, we use a method proposed by Varga and Lovas [34] who have shown that a fair approximation as given by

$$\sum_{\omega' R'} [N^{J\pi}_{\omega\omega'}(R,R') - \mu^{J\pi}_{ln} n^{J\pi}_{\omega\omega'}(R,R')] C^{J\pi}_{n\omega'}(R') = 0, \tag{21}$$

where $N^{J\pi}_{\omega\omega'}$ is the overlap GCM kernel (15) expressed in the pseudostate basis (10), and the matrix **n** is given by

$$n^{J\pi}_{\omega\omega'}(R,R') = \langle \Gamma_l(R) | \Gamma_l(R') \rangle \delta_{\omega\omega'}. \tag{22}$$

The overlap eigenfunctions are then obtained from

$$\chi^{J\pi}_{ln} = \sum_{\omega R} C^{J\pi}_{n\omega}(R) \Gamma_l(R). \tag{23}$$

In Fig. 7, we present the wave functions (18) for $J^\pi = 1/2^+$ and $1/2^-$ and for different energies. When a single generator coordinate R_C is included, $\omega=0$ only is, of course, allowed. In the full basis, $\omega=0$ concerns the ^{12}C(g.s.)$+n$ relative motion; the other values $\omega=1$ and $\omega=2$ correspond to pseudostates (their thresholds are located at more than 20 MeV).

In the two-center model, $J=1/2^-$ has no forbidden state, and $J=1/2^+$ has one forbidden state, yielding zero and one node, respectively, in the bound-state wave functions. The number of nodes is not modified in the multicluster approach, although forbidden states do not exist. For $J=1/2^-$, the ground-state wave function is weakly sensitive to distortion effects; at higher energies this sensitivity increases.

On the contrary, the $1/2^+$ wave functions are more sensitive to the ^{12}C description. This conclusion was already established from the analysis of the $B(E1,1/2^+ \rightarrow 1/2^-)$ values or from the proton width in ^{13}N. When the energy increases, the role of pseudostates is more and more important.

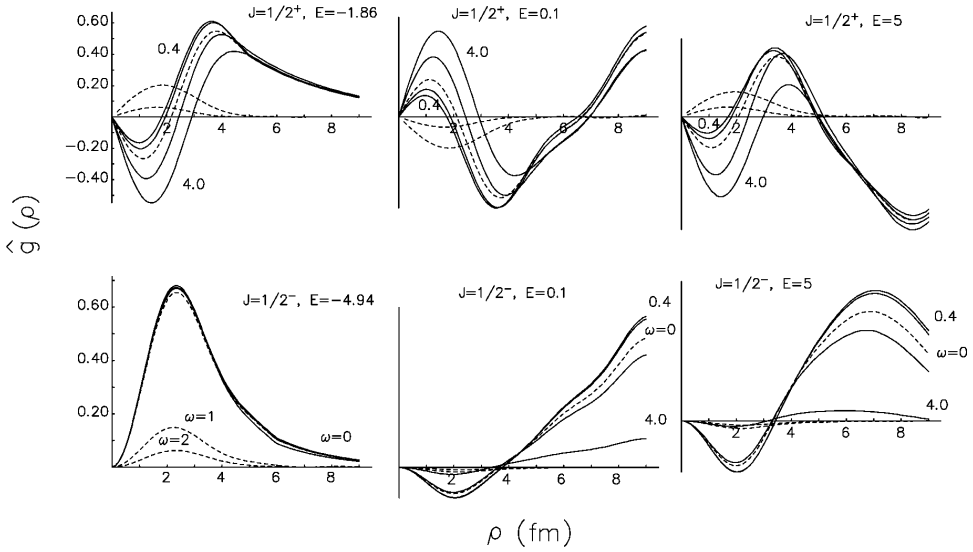

FIG. 7. ^{12}C+n relative wave functions [Eq. (18)] for bound states and scattering states at $E_{\text{c.m.}}=0.1$ and 5 MeV. The full curves correspond to the single R_C values. The dashed curves correspond to the multiconfiguration model. For the sake of clarity, only labels of $R_C=0.4$ and 4.0 fm are shown.

C. Radius of ^{12}C

From the approximate wave functions (17), it is possible to evaluate the rms radius of ^{12}C for a given ^{12}C+n distance ρ; one has

$$\langle R_{12}^2(\rho)\rangle = \frac{\sum_{\omega\omega'}\langle\phi_{12}^{\omega}|R_{12}^2|\phi_{12}^{\omega'}\rangle\hat{g}_{\omega}^{J\pi}(\rho)\hat{g}_{\omega'}^{J\pi}(\rho)}{\sum_{\omega\omega'}|\hat{g}_{\omega'}^{J\pi}(\rho)|^2}. \quad (24)$$

This quantity is plotted in Fig. 8. For large ρ values, it tends to the ^{12}C rms radius in its ground state. The ρ dependence of Eq. (24) arises from the pseudostates: if only $\omega=0$ is considered, Eq. (24) reduces to a constant. The role of the pseudostates is therefore to allow a ^{12}C distortion during the collision.

For $J^\pi=1/2^+$ whose wave functions present a node at small distance, there is an important variation of Eq. (24) near $\rho\approx 2$ fm. For $J^\pi=1/2^-$, and for positive energies in $J^\pi=1/2^+$, there are sharp variations close to the nodes. The pseudostates are characterized by large rms radii and yield an enhancement of Eq. (24) when $\hat{g}_0^{J\pi}(\rho)$ is negligible.

VI. CONCLUSION

We have analyzed clustering effects in the ^{12}C+n and ^{12}C+p systems. The multicluster approach includes deformation of ^{12}C during the collision. The spectroscopic properties of ^{13}C and ^{13}N are very sensitive to the ^{12}C description. More especially, the proton width of the $1/2^+$ resonance in ^{13}N and the $B(E1)$value between the $1/2^+$ and $1/2^-$ states require a strong deformation of ^{12}C. To investigate the sensitivity of the results with respect to the nucleon-nucleon interaction, we have used two different forces which have been demonstrated to give good accounts of data for other nuclei: V2 and Minnesota forces. In most cases, the sensitivity is fairly low, and lower than the sensitivity on R_C. The analysis of the ^{12}C$(p,\gamma)^{13}$N gives a good agreement with experiment, without any adjustable parameter. For ^{12}C$(n,\gamma)^{13}$C we reproduce the cross sections to different ^{13}C states in a reasonable way. A deeper investigation of the $1/2^+$ spectroscopy supports the existence of a halo structure in that state.

We also have studied deformation effects of ^{12}C in the ^{12}C+n system. Two typical partial waves have been chosen: the $1/2^-$ which does not present any node in the relative

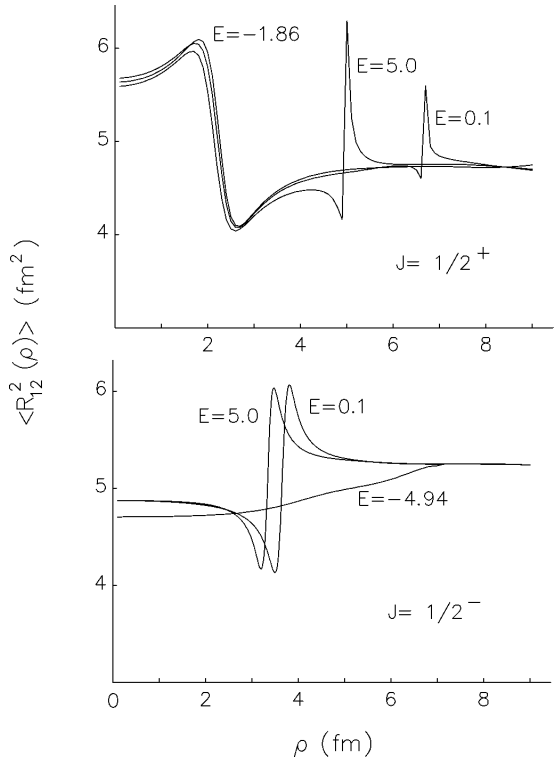

FIG. 8. Variation of the ^{12}C square radius as a function of the ^{12}C+n distance ρ [see Eq. (24)]. The curves are labeled by the c.m. energy.

wave function, and the $1/2^+$ partial wave which has one node. In the former case, deformation effects are rather weak, but in the latter the inner part of the wave function is strongly affected by ^{12}C clustering. This effect should be present in other reactions, such as $\alpha+^{12}C$, and perhaps enhanced if more nodes are involved in the wave functions. Further investigations in this direction are in the works.

This text presents research results of the Belgian program on interuniversity attraction poles initiated by the Belgian-state Federal Services for Scientific, Technical and Cultural Affairs.

[1] F. Ajzenberg-Selove, Nucl. Phys. **A523**, 1 (1991).
[2] R. G. Thomas, Phys. Rev. **88**, 1109 (1952).
[3] F. C. Barker and N. Ferdous, Aust. J. Phys. **33**, 691 (1980).
[4] C. Rolfs and W. S. Rodney, *Cauldrons in the Cosmos* (University of Chicago Press, Chicago, 1988).
[5] K. Langanke, O. S. Van Roosmalen, and W. A. Fowler, Nucl. Phys. **A435**, 657 (1985).
[6] Y. Nagai, M. Igashira, N. Mukai, T. Ohsaki, F. Uesawa, K. Takeda, T. Ando, H. Kitazawa, S. Kubono, and T. Fukuda, Astrophys. J. **381**, 444 (1991).
[7] T. Ohsaki, Y. Nagai, M. Igashira, T. Shima, K. Takeda, S. Seino, and T. Irie, Astrophys. J. **422**, 912 (1994).
[8] T. Otsuka, M. Ishihara, N. Fukunishi, T. Nakamura, and M. Yokoyama, Phys. Rev. C **49**, R2289 (1994).
[9] A. Mengoni, T. Otsuka, and M. Ishihara, Phys. Rev. C **52**, R2334 (1995).
[10] Y. C. Tang, *Topics in Nuclear Physics II,* Lecture Notes in Physics (Springer, Berlin, 1981), Vol. 145, p. 572.
[11] P. Descouvemont, Phys. Rev. C **47**, 210 (1993).
[12] M. Dufour, P. Descouvemont, and D. Baye, Phys. Rev. C **50**, 795 (1994).
[13] M. Dufour and P. Descouvemont, Nucl. Phys. **A605**, 160 (1996).
[14] D. Baye and P. Descouvemont, in *Proceedings of the 5th International Conference on Clustering Aspects in Nuclear and Subnuclear Systems*, Kyoto, Japan, 1988 [J. Phys. Soc. Jpn. **58**, 103 (1989)].
[15] P. Descouvemont, Phys. Rev. C **44**, 306 (1991).
[16] D. Brink, *Proceedings of the International School ''Enrico Fermi'' 36*, Varenna, 1965 (Academic Press, New York, 1966) p. 247.
[17] Y. Fujiwara, H. Horiuchi, K. Ikeda, M. Kamimura, K. Katō, Y. Suzuki, and E. Uegaki, Prog. Theor. Phys. Suppl. **68**, 29 (1980).
[18] D. Baye, P.-H. Heenen, and M. Libert-Heinemann, Nucl. Phys. **A291**, 230 (1977).
[19] H. Kanada, T. Kaneko, and Y. C. Tang, Nucl. Phys. **A380**, 87 (1982).
[20] D. Baye and M. Kruglanski, Phys. Rev. C **45**, 1321 (1992).
[21] A. B. Volkov, Nucl. Phys. **74**, 33 (1965).
[22] D. R. Thompson, M. LeMere, and Y. C. Tang, Nucl. Phys. **A286**, 53 (1977).
[23] F. Ajzenberg-Selove, Nucl. Phys. **A506**, 1 (1990).
[24] D. Baye and N. Pecher, Bull. Cl. Sc. Acad. Roy. Belg. **67**, 835 (1981).
[25] J. L. Vogl, Ph.D. thesis, California Institute of Technology, 1963.
[26] C. Rolfs and R. E. Azuma, Nucl. Phys. **A227**, 291 (1974).
[27] R. N. Hall and W. A. Fowler, Phys. Rev. **77**, 197 (1950).
[28] C. L. Bailey and W. R. Stratton, Phys. Rev. **77**, 194 (1950).
[29] W. A. S. Lamb and R. E. Hester, Phys. Rev. **107**, 55 (1957).
[30] G. R. Caughlan and W. A. Fowler, At. Data Nucl. Data Tables **40**, 283 (1988).
[31] T. Fliessbach and H. Walliser, Nucl. Phys. **A377**, 8 (1982).
[32] S. Saito, S. Okai, R. Tamagaki, and M. Yasuno, Prog. Theor. Phys. **50**, 1561 (1973).
[33] S. Saito, Prog. Theor. Phys. **41**, 705 (1969).
[34] K. Varga and R. G. Lovas, Phys. Rev. C **37**, 2906 (1988).